ANALYSIS OF FLOW STRUCTURES IN SUPERSONIC PLANE MIXING LAYERS WITH POD METHOD

Song Fu & Qin Yang*
School of Aerospace
Tsinghua University
Beijing 100084, China
fs-dem@tsinghua.edu.cn
qyang@nd.edu

ABSTRACT

The proper orthogonal decomposition (POD) method is applied to analyze the database obtained from the direct numerical simulation (DNS) of supersonic plane mixing layers. The effect of different forms of the inner products in the POD method is investigated. It is observed that the mean flow contributes to a predominant part of the total flow energy, and the energy spectrum of the turbulence fluctuations covers a wide range of POD modes. The patterns of leading (high energy) POD modes reveal that the flow structures exhibit spanwise counter rotating rolls, as well as oblique vortices. These flow patterns are insensitive to the velocity of the observer. As the convective Mach number increases, the energy spectrum becomes wider, the leading POD modes contain more complicated structures, and the flow becomes more chaotic.

INTRODUCTION

Turbulent flows are believed to be dominated by some large-scale coherent structures. For active control of turbulent flows of particular interest in many industrial applications, its important to describe the characteristics of the coherent structures correctly and to predict their evolution using the most simplistic procedure possible. Among many methods to investigate turbulent flow, proper orthogonal decomposition (POD) provides important insight. It extracts a certain number of mode functions, representative of the dominant structures, from a database of flow fields. It provides an optimal representation of a given set of flow field data and as such may be used to derive low-dimensional models.

Ever since the introduction of the POD method to fluid mechanics by Lumley (1967), it has been applied to many types of flows, especially shear-layer flows, such as boundary layers (Aubry et al., 1988), wakes (Ma et al., 2002), Couette flows (Meohlis at al., 2002), natural convections (He at al., 2003). and low-speed mixing layer (Deleville at al., 1999). In these studies, the flows have been mostly incompressible. It was found in these studies that a large percentage of the flow fields energy was captured by the first few leading modes. For an incompressible flow, velocities are the only dynamically important quantities. Using the POD method to decompose the velocity field leads to an induced norm of kinetic energy. However, for a compressible flow, both kinetic and thermodynamic variables are important, and should be included in certain forms of the inner product. Lumley et al. (1997) introduced a form of inner product, which added normalized velocity and density fluctuations in an optimal way, which we will be henceforth referring to as a normalized inner product. This form of the inner product is appropriate for homogeneous turbulence. Rowley et al. (2004) introduced a family of inner products that coupled the primitive variables in the isentropic Navier-Stokes equations, where the induced norm of that inner product has a physical interpretation of entropy. This family of inner products is applicable to moderately compressible flows. The differences between these two families of inner products are compared for the POD method of analysis as applied to supersonic mixing layers.

The supersonic mixing layer is a flow of great fundamental and practical importance. Good understanding of the flow behaviour is essential to the prediction of compressible turbulence and to the control of the mixing in supersonic flows. Ever since Brown and Roshko (1974) observed obvious large-scale spanwise rolls in plane mixing layers at low speeds (1974), it has been verified that mixing layers are dominated by these so-called Brown-Roshko vortices. Even in flows at moderately high Mach numbers, it is believed that the flow structures are dominated by compressibility rather than by viscosity (Clements et al., 1995). As compressibility increases, the mixing layer contains structures that are more three-dimensional and obliquely oriented (Leep et al., 1993), and the typical Brown-Roshko rolls seem to merge with the rest of the flow. In the fully developed turbulent region, our knowledge of the large-scale coherent structures is still rather limited. This study attempts to identify these flow structures in a compressible, fully developed turbulent mixing layer by applying the POD method to a comprehensive DNS database from the work of Li et al. (2002) (See also Fu et al., 2006).

PROPER ORTHOGONAL DECOMPOSITION

POD Method basics

The central idea of the POD method is to determine a set of basis functions $\{\phi_i | i = 1, \ldots, \infty\}$ that optimally span the data ensemble $\mathbf{q}^k \in L^2(\Omega) | k = 1, \ldots, M\}$, in the sense that the error of the projection onto be basis set is minimized. This objective is equivalent the following optimization problem,

$$\max_{\phi \in L^2(\Omega)} \frac{\langle |(\mathbf{q}, \phi)|^2 \rangle}{\|\phi\|^2}, \tag{1}$$

where $L^2(\Omega)$ is an L^2 space of functions on some spatial domain Ω with the inner product $(\cdot, \cdot)$, $\|\cdot\|$ is the induced norm on $L^2(\Omega)$, and $\langle \cdot, \cdot \rangle$ denotes the ensemble average over k. The

*currently at: Hessert Center of Aerospace Research, Dept. of Aero. & Mech. Engr., University of Notre Dame, IN 46556, U.S.

data $\{\mathbf{q}^k\}$ could be thought of as a data ensemble of different experiments, or of snapshots at different times. Solving this optimization problem using the variational method leads to an eigenvalue problem,

$$\Re\phi = \lambda\phi, \tag{2}$$

where $\Re : L^2(\Omega) \rightarrow L^2(\Omega)$ is a linear integral operator given by

$$\Re\phi = \int_\Omega \langle \mathbf{q}^k \otimes \mathbf{q}^{k*} \rangle \phi d\mathbf{x}. \tag{3}$$

Here the symbol $*$ denotes the complex conjugate, and $\otimes$ is the usual tensor product. It follows from the definition shown in (3) that $\Re$ is self-adjoint and non-negative definite, therefore it's eigenfunction ϕ is indeed orthonormal. The set $\{\phi_i\}$ is complete in the sense that $\{\mathbf{q}^k\}$ can be represented as a series expansion of the orthonormal basis,

$$\mathbf{q}^k = \sum_{i=1}^{\infty} {a_i}^k \phi_i, \tag{4}$$

where ${a_i}^k = (\mathbf{q}^k, \phi_i)$.

The non-negative definition of the operator $\Re$ also ensures that all eigenvalues λ_i are non-negative. Furthermore, it can be seen that the inner product between $\{\mathbf{q}^k\}$ and ϕ_i is

$$\lambda_i = \langle |(\mathbf{q}^k, \phi_i)|^2 \rangle. \tag{5}$$

Here, the eigenvalue λ_i is the average "energy" in the projection of the ensemble $\{\mathbf{q}^k\}$ onto ϕ_i. By realigning ϕ_i in decreasing order of the corresponding eigenvalues $\lambda_1 > \lambda_2 > \cdots > \lambda_n$, the ratio λ_i over the sum $\sum_i \lambda_i$ can be written as

$$E_i = \frac{\lambda_i}{\sum_i \lambda_i}, \tag{6}$$

which reflects the fraction of the totally energy contained in the ith mode.

Thus, if the subspace is expanded with the eigenfunctions $\{\phi_i | i = 1, \cdots, N\}$ corresponding to the large-to-small eigenvalues, then the representation

$$\hat{\mathbf{q}}^k = \sum_{i=1}^{N} {a_i}^k \phi_i \tag{7}$$

contains a percentage of the total energy given by $\sum_{i=1}^{N} E_i$, representing the most "energetic" reduced-order form of the original dataset. the eigenfunctions ϕ_i are called eigenmodes or POD modes. The POD method literally reflects the mathematics of this equation. For more detailed discussion on the POD method one can refer to Lumley et al. (1996).

It is worth noting that the order of the eigenvalue problem (1) can be very high. As we know, a high resolution experimental database or DNS dataset usually contains information for a large number of elements. Assuming $\mathbf{q}$ is a J component vector field on a domain with K elements and the eigenvalue problem (1) is directly solved, then $\Re$ turns out to be of the order $J \times K$. For the 3D DNS dataset investigated here, the number of elements $K \approx 400,000$, thus it is impractical to work with such a large eigensystem. In order to circumvent this difficulty, a snapshot method was adopted.

Snapshots Method

The snapshot method introduced by Sirovich (1987) provides an alternative way to implement the POD method. The key step of the snapshot method is to represent the POD modes by a linear combination of the flow field data $\mathbf{q}^k$, where k represents an independent series of time steps which can be seen as snapshots of the flow field. This can always be achieved since the range of $\Re$ is contained within the span of the ensemble $\{\mathbf{q}^k \in L^2(\Omega) | k = 1, \cdots, M\}$. Following this idea, any eigenfunction ϕ_i can be written as

$$\phi_i = \sum_{k=1}^{M} {A_i}^k \mathbf{q}^k, \tag{8}$$

where M is the number of snapshots. Substituting (4) into (1), and defining $\langle \cdot \rangle$ as an average over k, we obtain the algebraic eigenvalue equation

$$\mathbf{CA} = \lambda\mathbf{A}, \tag{9}$$

where $C_{ij} = (\mathbf{q}^i \mathbf{q}^j)/M$and $A_i = ({A_i}^1, {A_i}^2, \cdots {A_i}^M)$ is the eigenvector corresponding to the ith eigenvalue λ_i. Here i and j increase as $i, j = 1, 2, \cdots, M$. Thus, one can obtain the POD eigenmodes by solving an eigenvalue equation of order M. Typically, M is not a large number in comparison to the grid size of the domain. In our DNS database, the snapshot number is of $O(10^2)$, which is much smaller than the value $J \times K$ mentioned in the previous section. Therefore, in order to solve the eigenvalue problem more efficiently, the snapshot method was adopted to obtain the POD modes in the present study.

The POD Vector and Inner Product

When applying the basic theory described above to a flow problem, the normed space on which the POD method is applied should be chosen to best suit the problem, namely, the vector field q, and the inner product on the field. In the following discussion, we will refer to these as a POD vector and an inner product.

For an incompressible flow, where velocity is the only dynamically important quantity, the natural choice for the POD vector field is

$$\mathbf{q}_k(\mathbf{x}) = (u(\mathbf{x}, k\tau), v(\mathbf{x}, k\tau), w(\mathbf{x}, k\tau)), \mathbf{x} \in \Omega, \tag{10}$$

where u, v and w are the streawise, transverse and spanwise components of the velocity, respectively. The spatial coordinate vector is denoted by $\mathbf{x}$ and the time step between two consecutive snapshots is given by τ. Thus the standard inner product is written as:

$$(\mathbf{q}_1, \mathbf{q}_2) = \int_\Omega (u_1 u_2 + v_1 v_2 + w_1 w_2) d\mathbf{x}, \tag{11}$$

where the optimization criterion for the POD method (Eq. (1)) becomes kinetic energy. In this way, the POD method extracts the flow information containing the most kinetic energy in a time-averaged sense.

If the vorticity vector $\mathbf{q} = (\omega_x, \omega_y, \omega_z)$ is adopted as a POD vector, and the inner product is chosen in the standard way (such a choice may be suitable for some flows, see Kostas et al. 2005), the leading POD modes represent flow structures that contain the most enstrophy in a time-averaged sense.

In a supersonic flow, compressibility plays a crucial role and, as such, all the kinetic and thermodynamic variables should be included in the normed space for the POD analysis. The choice of inner product is no longer trivial. For

instance, if the POD vector $\mathbf{q} = (\rho, u, v, w)$ is employed, with ρ representing the density, then the standard inner product would lead to an induced norm without any physical meaning, since one cannot add velocity and density together.

One can, of course, process all variables of interest separately, which means several variables are not bundled together in a vector-valued space, but rather put into several scalar-valued fields on which the POD method is performed separately. This is applicable when we are interested in a single variable, which can describe a particular flow pattern sufficiently. For instance, we can define $\mathbf{q} = p$, with p representing the pressure, which is the descriptive quantity for some compressible flows, so that the leading POD modes demonstrate the main pattern of pressure distributions. In this way, the lack of physical interpretation of the induced norm is obvious, and no dynamical interaction between different quantities can be included.

Rowley et al. (2004) introduced a family of inner products, which couple all the primary variables in the isentropic Navier-Stokes equations, while also providing a direct physical interpretation for the induced norm. In Rowleys method, assuming isentropic flow conditions, the continuum equation is reduced to an equation used to solve for the local sound speed c. Thus, the POD vector is defined by $\mathbf{q} = (u, v, w, c)$ with inner product of the form

$$(\mathbf{q}_1, \mathbf{q}_2) = \int_\Omega (u_1 u_2 + v_1 v_2 + w_1 w_2 + \frac{2}{\gamma - 1} c_1 c_2) d\mathbf{x}. \quad (12)$$

The induced norm takes the form of twice the total enthalpy $h = \frac{1}{2}(u^2 + v^2 + w^2) + \frac{c^2}{\gamma - 1}$. This physical meaning of the induced norm assures us that the leading POD modes can be related to the structure that contains the largest portion of total enthalpy. Because this inner product couples all the primary variables in the isentropic Navier-Stokes equations, it becomes straightforward to deduce a low-dimensional dynamical system from the obtained POD modes. An energy-based inner product is preferred because it retains the stable equilibrium points at the origin in the low-dimensional model. Applying this method to flows at moderately high Mach numbers has generated satisfactory results (Mereno et al., 2004). Equations (11) and (12) will be referred to as energy-based inner products in the following discussion.

Lumley et al. (1997) suggested a way of coupling velocity and pressure together through nondimensionalization. The velocity and density is nondimensionallized and weighted optimally in the sense that the eigenvalue λ is largest for a given choice of eigenmodes ϕ. The nondimensionalized POD vector is as

$$\mathbf{q} = \left(\frac{\rho'}{\langle \rho'^2 \rangle^{\frac{1}{2}}}, \frac{u'}{\langle \mathbf{v}'^2 \rangle^{\frac{1}{2}}}, \frac{v'}{\langle \mathbf{v}'^2 \rangle^{\frac{1}{2}}}, \frac{w'}{\langle \mathbf{v}'^2 \rangle^{\frac{1}{2}}} \right). \quad (13)$$

Here, the symbol $'$ denotes the fluctuating component of a variable, and $\overline{\langle \cdot \rangle}$ denotes the average over time and space. Now the standard inner product takes the form

$$(\mathbf{q}_q 1, \mathbf{q}_2) = \int_\Omega \left(\frac{\rho_1' \rho_2'}{\overline{\langle \rho'^2 \rangle}} + \frac{u_1' u_2' + v_1' v_2' + w_1' w_2'}{\overline{\langle \mathbf{v}'^2 \rangle}} \right) d\mathbf{x}, \quad (14)$$

Similarly, if the fluctuating temperature T' is also included in the POD vector, one can obtain

$$(\mathbf{q}_1, \mathbf{q}_2) = \int_\Omega \left[\frac{\alpha}{2} \left(\frac{\rho_1' \rho_2'}{\overline{\langle \rho'^2 \rangle}} + \frac{u_1' u_2' + v_1' v_2' + w_1' w_2'}{\overline{\langle \mathbf{v}'^2 \rangle}} \right) + (1 - \alpha) \frac{T_1' T_2'}{\overline{\langle T'^2 \rangle}} \right] d\mathbf{x}, \quad (15)$$

Table 1: Basic Parameters for DNS Dataset.

Case No	Ma_c	Ma_1	Ma_2	Re_c	M
3D-1	0.4	1.9	1.1	375	300
3D-2	0.8	2.9	1.3	525	300
3D-3	1.2	3.9	1.5	575	300

where $0 < \alpha < 1$, which is a constant parameter that adjusts the weighting ratio between temperature and other variables. This form of inner product works well with homogeneous turbulence, providing a set of POD basis to deduce low-dimensional dynamic systems from fully compressible Navier-Stokes equations, by coupling the primary variables. Equations (14) and (15) will be referred to as weighted inner products in the following discussion.

IMPLEMENTATION OF POD

DNS Database

The investigation is based on several sets of flow data obtained from DNS of the fully compressible Navier-Stokes equations (Li et al. 2002; Fu et al. 2006). Included in these sets are a 2D simulation with convective Mach number $Ma_c = 0.4$ and 3D simulations with $Ma_c = 0.4$, 0.8, and1.2. The parameters used in these 4 simulations are listed in Table 1, where subscripts 1 and 2 denote the parameters of the high-speed and low-speed parts of the mixing layer, respectively. The convective Mach number is given by $Ma_c = (U_1 - U_2)/(c_1 + c_2)$ where U and c are the velocity and sound speed of the mean flow and $Re_c = (U_1 + U_2)\delta_m/(2\nu)$ is the convective Reynolds number with δ_m representing the momentum thickness and ν the kinetic viscosity.

All of the variables are nondimensionalized by the initial vorticity thickness $\delta_\omega(0)$, the free stream density $\rho_\infty = \rho_1 = \rho_2$, and the free stream sound speed $c_\infty = c_1 = c_2$. The snapshots are taken at evenly spaced points in time after the initial transients have decayed, encompassing the span of time over which a disturbance travels through the computational domain.

Effects of Inner Products

In this section we compare the results for several different choices of normed spaces discussed above to the case 3D-1, with the aim of determining an appropriate way of extracting structures that contain the most energy of a supersonic mixing layer. The results obtained for different choices of inner products in POD are shown in Figs. 1 and 2. Both figures shows distinct differences between the results produced by the weighted inner products Eqs. (14) and (15), and the energy-based inner products Eqs. (11) and (12). The weighted inner products produce higher energy concentration and less integrated and organized structures in the leading modes than those generated by the energy-based inner products. However, differences of results generated by inner products belonging to the same category are subtile.

This suggests there is actually no best way to determine a configuration space for the POD method. The choice of configuration space is dependent upon the desired method of filtering, with the aim of obtaining the leading POD modes representative of the large-scale structures in the flow field.

Mean Flow Effect

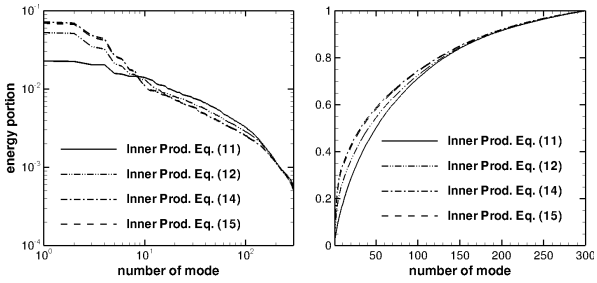

(a) (b)

Figure 1: "Energy" distribution obtained from inner products Eq. (11), (12), (14) and (15): (a) in each POD mode; (b) in a number of leading modes.

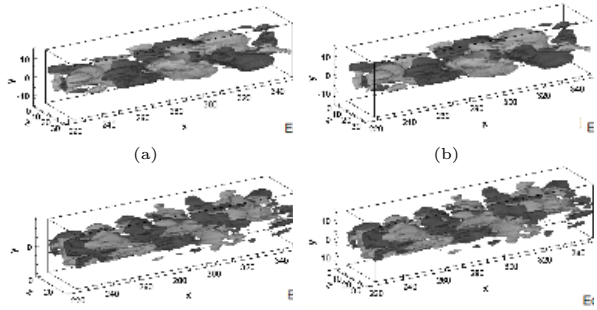

(a) (b) (c) (d)

Figure 2: Fluctuation streamwise velocity iso-surfaces for the 1st order POD modes obtained from inner products (a) Eq. (11), (b) Eq. (12), (c) Eq. (14) and (d) Eq. (15).

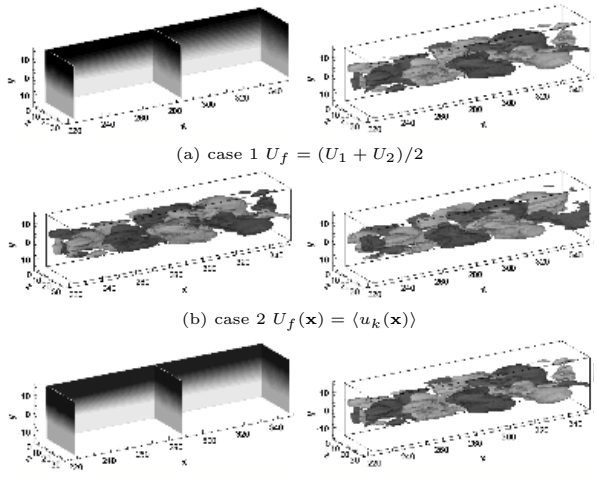

(a) case 1 $U_f = (U_1 + U_2)/2$

(b) case 2 $U_f(\mathbf{x}) = \langle u_k(\mathbf{x}) \rangle$

(b) case 3 $U_f = 0$

Figure 3: Fluctuation streamwise velocity contour/iso-surfaces for the POD modes of 1st order (left), and the 2nd order (right) obtained from inner products (a) Eq. (11), (b) Eq. (12), (c) Eq. (14) and (d) Eq. (15).

The coherent structures, depicted by the velocity field, often change their shape with respect to the velocity of the observer. In order to examine how much the POD modes change according to the reference velocity, the DNS data was subtracted by different reference flow U_f. The results showed that when $U_f = (U_1 + U_2)/2$ (case 1), the first POD mode captures about 84% of the total energy, when $U_f(\mathbf{x}) = \langle u_k(\mathbf{x}) \rangle$ (case 2), where $\langle \cdot \rangle$ stands for average over snapshots k, the first POD modes captures only about 2.3% of the total energy, while for the original data, the first POD mode captures more than 99% of the total energy (case 3). For the 3 cases, the energy convergences after the 1st order mode are all quite slow, with a dropping of magnitude of $O(10^{-1})$ over more than 100 modes. Figure 3 shows the first 2 POD modes for each of the three cases. This results suggest that the first POD modes in case 1 and 2 are basically the mean flow, which contains most of the energy in the mixing layer. And the shape of POD modes for the fluctuations is not quite sensitive to the choice of the reference flow. so the focus of this study is on the field of fluctuations.

POD ANALYSIS OF FLOW STRUCTURES

In the following analyses, the inner product of Eq. (15) for the fluctuation field is applied. The most significant difference among the three cases lies in their compressibility, which is denoted by the convective Mach numbers Ma_c. The convective Mach numbers of the flows relate directly to the characteristics of their coherent structures.

Figure 4 shows that the energy spectrums of the 3 cases of 3D mixing layers cover a wide range of POD modes. For case 3D-1($Ma_c = 0.4$) and 3D-2($Ma_c = 0.8$), the leading 50 modes take less than 60% of the total fluctuation energy, while for case 3D-3($Ma_c = 1.2$), the first 50 modes take less than 50% of the total fluctuation energy. This is an indication that these flows are all highly turbulent.

Figure 5 shows the coefficients of several POD modes. These coefficients represent the transient energy extracted by their corresponding POD modes (see Eq. (7)). They also graph how the structures associated with each POD mode evolve over time. In Fig. 5, the coefficients of low order modes form pairs, showing good regularity, quasi-periodicity and hence, coherence of large scale structures; while the coefficients of high order modes behave rather randomly.

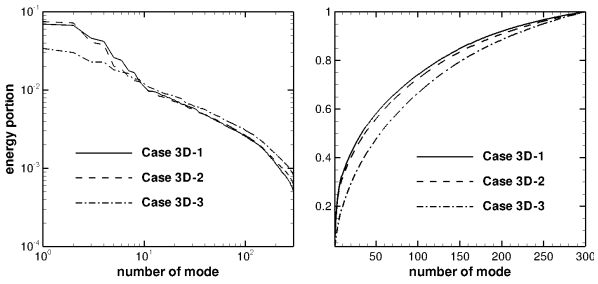

(a) (b)

Figure 4: "Energy" distribution of case 3D-1, 3D-2 and 3D-3 obtained from inner products Eq. (15): (a) in each POD mode; (b) in a number of leading modes.

Comparison among the three cases reveals that, as Ma_c goes up, the period of the evolution of the coefficients becomes longer, indicating a growing time scale of the movement of the large-scale structures with increased level of compressibility. Additionally, as Ma_c increases, the time evolution of high-order mode coefficients also increases in their regularity. In fact, Fig. 4 provides a very good indication that the coherent structures exist in supersonic mixing layers though the structure scale may be much smaller than those in incompressible cases.

Figures 5, 6 and 7 show the POD modes of the 1st, 2nd, 15th and 60th order of the three 3D cases respectively. In these figures, the two leading modes occur in pairs, shifted by a phase of roughly 90°. The density iso-surfaces of leading modes show the form of propagating waves. The streamlines of leading modes form a streamwise array of spanwise counter rotating rolls similar to the Brown-Roshko vortices.

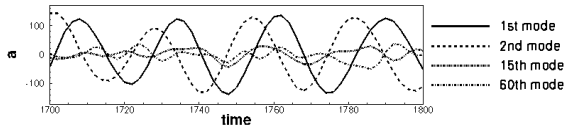

(a) Case 3D-1

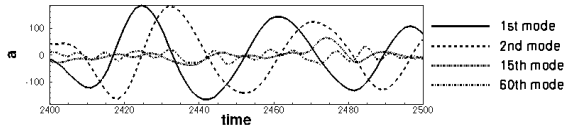

(b) Case 3D-2

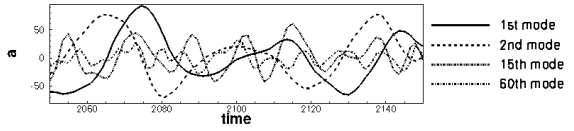

(c) Case 3D-3

Figure 5: Time evolution of instantaneous "energy" projected on the 1st, 2nd, 15th and 60th POD mode in three 3D cases.

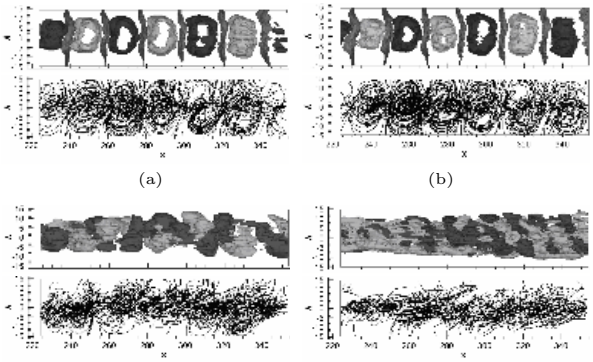

(a) (b)

(c) (d)

Figure 6: Iso-sufaces of fluctuation density (upper plots) and streamlines (lower plots) viewed from the spanwise direction for (a) the 1st, (b) 2nd, (c) 15th and (d) 60th POD modes obtained by inner product Eq.(15) from case 3D-1.

However, it is obvious that these structures do not play a dominant role in the flow. As seen from the previous discussion, the leading modes of the fluctuation field capture only a small portion of the total energy. As the order of POD modes increases, the structures of spanwise rolls break down gradually becoming more and more oblique in the streamwise direction. This can be interpreted as a significant amount of streamwise flow pattern being contained in the small-scale structures, although they are basically convoluted.

Comparison of Figs. 5, 6 and 7 shows the effect of flow compressibility on the pattern of POD modes. It is observed that as the Ma_c goes up, the scale of the length of the structure for each mode increases, which is obviously shown by lower order POD modes. This trend suggests that the mixing layer becomes energized with increased compressibility.

The coherent flow structures depicted in the previous figures can be further demonstrated by applying POD to the vorticity field. Figure 9 shows the spanwise and streamwise components of vorticity for POD mode of the 1st order. The 1st order POD mode of streamwise voticity, which corresponds to spanwise rolls shown by streamlines in Fig. 6, indicates a large scale of alternating positive and negative vorticity patterns. Within these alternating patterns, streamwise structures play a dominant role. The complex alternating and streamwise structures are also evident in the POD mode of streamwise vorticity ω_x. The streamwise

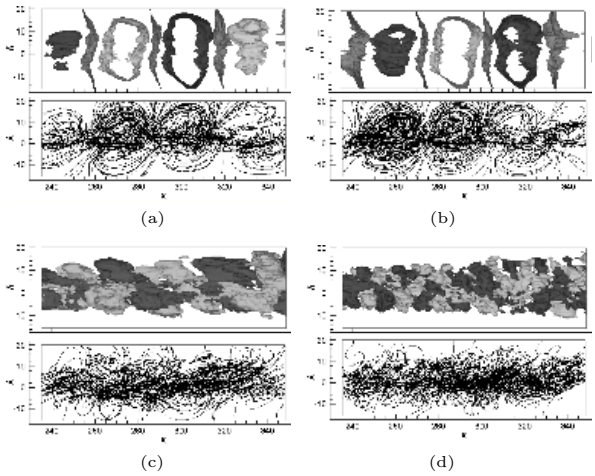

(a) (b)

(c) (d)

Figure 7: Iso-surfaces of fluctuation density (upper plots) and streamlines (lower plots) viewed from the spanwise direction for (a) the 1st, (b) 2nd, (c) 15th and (d) 60th POD modes obtained by inner product Eq.(15) from case 3D-2.

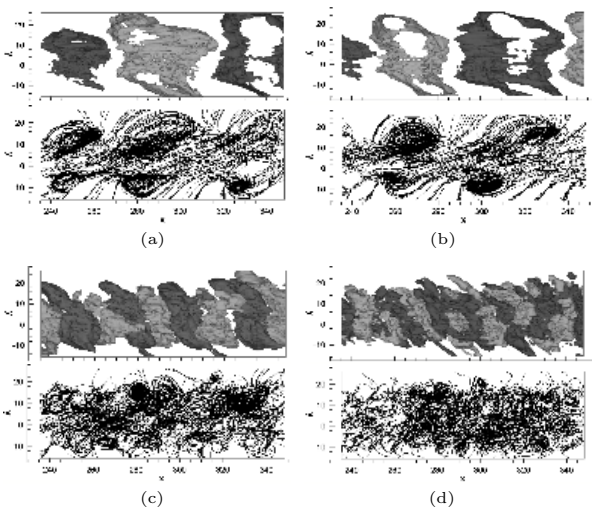

(a) (b)

(c) (d)

Figure 8: Iso-surfaces of fluctuation density (upper plots) and streamlines (lower plots) viewed from the spanwise direction for (a) the 1st, (b) 2nd, (c) 15th and (d) 60th POD modes obtained by inner product Eq.(15) from case 3D-3.

structures are smoother while the alternating patterns are less clear than those in the spanwise voticity. As pointed out earlier, the alternating patterns reflect the 2-D rolling structures shown in the density contours in Figs. 6-8, hence, they are mainly spanwise in orientation and better represented by the spanwise vorticity ω_z. Meanwhile, the streamwise vorticity ω_x is also an appropriate candidate for the representation of the flow structures.

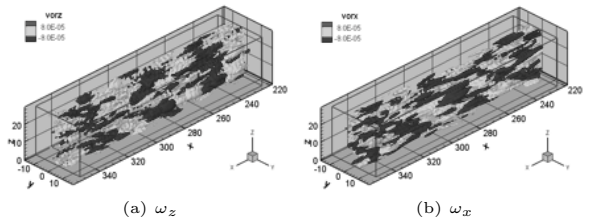

(a) ω_z (b) ω_x

Figure 9: Iso-surfaces of the 1st order POD mode of spanwise and streamwise vorticity for case 3D-1.

CONCLUSION

Supersonic mixing layers with moderately high Ma_c values in the fully developed turbulent region, where self-similarity is preserved, have been known to exhibit highly random and three-dimensional flow structures. It was not clear if there were any large-scale coherent structures in the high-speed cases similar to the Brown-Roshko roller type existing in low-speed mixing layers. The present study was aimed at investigating the flow structures from DNS data for supersonic mixing layers with the aid of the POD method.

The effect of the inner products on the POD method analysis was examined first. Although there has been discussion in literature concerning appropriate forms for the inner products in the POD method, it was shown in this work that the inner product does not significantly affect the resulting POD mode patterns nor energy distributions. However, the energy-based inner products generate less concentrated energy distributions and clearer low-order mode shapes in comparison to the weighted inner products.

This POD analysis shows coherent structures exist in supersonic mixing layers for each of the three convective Mach number cases studied. A few leading POD modes exhibit similar structures and spanwise counter-rotating rolls behaviours as those in the incompressible mixing layer but on a much smaller scale as compared to the remaining turbulence. The main difference between the incompressible and compressible mixing layers lies in the energy spectrum of the POD modes. In the former case the leading POD modes represent most of the turbulence energy while in the latter the first 10 POD modes account for less than 18% of the total energy. Therefore it would be difficult to reconstruct the flow field using only the first few modes, as is done in low-dimensional modelling. Furthermore, the spanwise rolling structures were observed to contain streamwise flow patterns.

As the convective Mach number increases, the flow becomes more complex, causing the energy spectrum over the POD modes to become wider and less concentrated in low order modes. The coherent structures also become more and more oblique in the streamwise direction, indicating enhanced streamwise structures. It should be mentioned that the POD modes representative of the large-scale structures in the fluctuations of the supersonic mixing layer do not change much according to the velocity of an observer, or whether or not the mean flow is included in the analysis.

ACKNOWLEDGEMENTS

This work was supported by the National Natural Science Foundation of China (Grant No. 10232020, 90505005). We thank our colleague Dr. Qibing Li for his very helpful discussions, Ms. Alice Nightingale and Mr. Robert Sproston for proofreading this paper.

REFERENCES

Aubry, N., Holmes, P., Lumley, J. L., Stone, E., 1998, "The Dynamics of Coherent Structures in the Wall Region of a Turbulent Boundary Layer", *Journal of Fluid Mechanics*, Vol. 192, pp. 115-173.

Brown, G. L., Roshko, A., 1974, "On Density Effects and Large Structure in Turbulent Mixing Layers", *Journal of Fluid Mechanics*, Vol. 64, pp. 775-816.

Clemens, N. T., Mungal, M. G., 1995, "Large-Scale Structrures and Entrainment in the Supersonic Mixing Layer", *Journal of Fluid Mechanics*, Vol. 284, pp. 171-216.

Delville, J., Ukeiley, L. et al., 1999, "Examination of Large-scale Structures in a Turbulent Plane Mixing Layer", *Journal of Fluid Mechanics*, Vol. 391, pp. 91-122.

Fu, S. and Li, Q., 2006, "Numerical simulation of compressible mixing layers", *International Journal of Heat and Fluid Flow*, Vol. 03, pp. 028

He, J., Fu, S., 2003, "POD Analysis of Large-Scale Coherent Structures in Turbulent Thermal Convection", *Acta Mechanica Sinica (in Chinese)*, Vol. 35(4), pp. 385-392.

Holmes, P. J., Berkooz, G., and Lumley, J. L., 1996, "Turbulence, Coherent Structures, Dynamical Systems and Symmetry", Cambridge: Cambridge University Press.

Kostas, J., Soria, J. and Chong, M. S., 2005, "A Comparison between Snapshot POD Analysis of PIV Velocity and Vorticity Data, *Experimental Fluids*, Vol. 38, pp. 146-160.

Leep, L. J., Dutton, J. C., Burr, R. F., 1993, "Three Dimensional Simulations of Compressible Mixing Layers: Visualizations and Statistical Analysis, *AIAA Journal*, Vol. 31, pp. 2039-2046.

Li, Q., 2002, "Numerical Study of Compressible Mixing Layer with BGK Scheme", Ph.D. Thesis, Tsinghua University, Beijing, China.

Lumley, J. L., 1967, "The Structure of Inhomogeneous Turbulence", *Atmospheric Turbulence and Wave Propagation*, Yaglom, A. M., Tatarski V. I., ed., Nauka, Moscow, pp. 166-178.

Lumley, J. L., Poje, A., 1997, "Low-Dimensional Models for Flows with Density Fluctuations", *Physics of Fluids*, Vol. 9(7), pp. 2023-2031.

Ma, X., Karniadakis, G., 2002, "A Low-Dimensional Model for Simulating Three-Dimensional Cylinder Flow", *Journal of Fluid Mechanics*, Vol. 458, pp. 181-190.

Mereno, D., Krothapalli, A., Alkislar, M. B., Lourenco, L. M., 2004, "Low-dimensional Model of a Supersonic Rectangular Jet", *Physical Review E.*, Vol. 69, pp. 026304.

Moehlis, J., Smith, T. R., Holmes, P., Faisst H., 2002, "Models for Turbulent Plane Couette Flow Using the Proper Orthogonal Decomposition", *Physics of Fluids*, Vol. 14(7), pp. 2493-2507.

Rowley, C. W., Colonius, T., Murray, R. M., 2004, "Model Reduction for Compressible Flows Using POD and Galerkin Projection", *Physica D*, Vol. 189, pp. 115-129.

Sirovich, L., 1987, "Turbulent and the Dynamics of Coherent Structures, Parts I-III", *Quarterly of Applied Math*, Vol. XLV(3), pp. 561-582.